electronics

MDPI

Article

Advanced Design and Implementation of a 2-Channel, Multi-Functional Therapeutic Electrical Stimulator

Rujira Lakatem, Suttipong Boontaklang and Chow Chompoo-inwai *

Department of Electrical Engineering, School of Engineering, King Mongkut's Institute of Technology Ladkrabang, Bangkok 10520, Thailand; 63601024@kmitl.ac.th (R.L.); suttipong.boon@gmail.com (S.B.)
* Correspondence: chow.ch@kmitl.ac.th

Abstract: This research introduces the design, implementation, and rigorous evaluation of a novel 2-channel, multi-functional therapeutic electrical stimulator, meticulously engineered to meet the stringent demands of contemporary clinical applications. The device integrates a high-speed R-2R ladder DAC and a sophisticated pulse generator unit, capable of producing twelve essential current waveforms with fully adjustable parameters, including pulse amplitude, pulse duration, and pulse repetitive frequency. The proposed driving stage unit ensures precise voltage-to-current conversion, delivering stable and accurate output currents even under varying load conditions, which effectively simulate the diverse impedance characteristics of human tissue. Extensive testing confirmed the compliance with international medical standards, notably IEC 60601-1, IEC 60601-1-2, and IEC 60601-2-10. The experimental results underscore the device's consistent operation within prescribed safety and performance thresholds, with all deviations in pulse parameters remaining well below the permissible limits. Furthermore, the proposed electrical stimulator demonstrated exceptional stability across variable load conditions, as evidenced by minimal amplitude errors and high correlation between waveform characteristics. These findings highlight the proposed device's robustness and its potential as a versatile tool for a wide range of therapeutic applications, including pain management, muscle stimulation, and nerve rehabilitation, thus marking a significant advancement in the field of therapeutic electrical stimulation.

Keywords: therapeutic electrical stimulator; pulse generator unit; driving stage unit; multi-functional stimulator; IEC 60601-1; IEC 60601-1-2; IEC 60601-2-10

Citation: Lakatem, R.; Boontaklang, S.; Chompoo-inwai, C. Advanced Design and Implementation of a 2-Channel, Multi-Functional Therapeutic Electrical Stimulator. *Electronics* **2024**, *13*, 3793. https://doi.org/10.3390/electronics13193793

Academic Editor: Luca Mesin

Received: 21 August 2024
Revised: 17 September 2024
Accepted: 21 September 2024
Published: 24 September 2024

1. Introduction

Electrical Stimulation (ES) is a widely recognized therapeutic technique that applies electrical impulses to stimulate nerves, muscles, or tissues. Historically, ES devices have played a significant role in clinical settings, particularly in physiotherapy and rehabilitation. Their initial application primarily targeted aging populations to address conditions such as muscle atrophy, pain management, and mobility enhancement [1]. However, in recent years, the scope of ES has expanded significantly beyond this demographic.

Today, younger generations increasingly benefit from ES technology due to modern lifestyle factors such as muscle injuries, office syndrome, and conditions associated with prolonged sitting, such as neck and back pain. This growing demand demonstrates the versatility of ES in addressing various medical conditions and highlights its importance across a broader age spectrum. As a result, ES has emerged as a vital tool not only for therapeutic applications but also for preventive care, with its relevance expected to expand further in the coming years. This shift underscores the necessity for adaptable, efficient, and user-friendly ES devices to meet the evolving needs of diverse populations.

The continuous expansion of ES applications has driven significant technological advancements. Since its first recorded use in 1791, ES has become integral to treatments such as physiotherapy, pain relief, muscle strengthening, cardiac pacing, iontophoretic

drug delivery, and functional electrical stimulation (FES) [1,2]. The introduction of the first commercially available ES device in 1969, which facilitated motor function recovery [3], marked the beginning of rapid technological evolution. These developments have since paved the way for more sophisticated and versatile devices suitable for both clinical and non-clinical applications [1–21].

Modern ES devices generate a variety of waveforms, including square, rectangular, sinusoidal, triangular, and Gaussian shapes. These waveforms are often given specific technical names within therapeutic settings; for example, rectangular waveforms are referred to as faradic waves, while sinusoidal waveforms are known as diadynamic waves [22]. The therapeutic outcomes of ES are highly dependent on parameters such as pulse amplitude, pulse duration, pulse frequency, and polarity [23]. Customizing these parameters allows ES devices to target specific treatment goals, significantly enhancing their effectiveness in treating a wide range of medical conditions.

ES devices can be categorized based on several criteria: the mode of application (surface vs. implanted stimulators) [24], the type of waveform (monophasic or biphasic), and the clinical application (e.g., Neuromuscular Electrical Stimulation (NMES), Functional Electrical Stimulation (FES), or Transcutaneous Electrical Nerve Stimulation (TENS)) [25]. The flexibility to generate diverse waveforms with varying durations and frequencies is critical to the adaptability of ES devices in therapeutic contexts, thereby improving clinical outcomes [26].

The core components of ES devices include the user interface (UI), controller, pulse generator, and driving stage/output circuit [1,3–7,10,12–18,20,25]. The UI translates user inputs into parameters for waveform generation, the controller manages system operations, the pulse generator creates the waveforms, and the driving stage amplifies these waveforms into output currents delivered to the target tissues. While this study focuses primarily on the pulse generator and driving stage—as they play pivotal roles in ensuring the precision and efficacy of the ES device—the UI and controller will not be discussed in detail in this paper.

One of the key challenges in designing ES devices is generating non-linear signals for various stimulation patterns. Early analog pulse generators were limited in flexibility, providing fixed waveform parameters [1]. The advent of digital microcontrollers (MCUs) enabled the programmable generation of waveforms, offering greater control for multi-channel and multi-functional devices [24]. However, generating precise signals remains a challenge due to memory constraints [2,7] and real-time processing limitations in MCUs [1,4]. This study addresses these issues by exploring a real-time synthesizing approach that bypasses traditional Look-Up Tables (LUTs) [5], enabling more efficient waveform generation with higher resolution and minimal distortion.

Another critical challenge in ES design is converting digital signals into analog form. Traditional Digital-to-Analog Converters (DACs) are commonly used with MCUs to generate the necessary output signals [1,4,5,10,12,20]. However, typical DAC chips have limitations in terms of output range, customization, and speed, all of which are crucial for generating non-linear signals [27,28]. To overcome these limitations, this study proposes the use of a discrete R-2R ladder DAC circuit, which provides higher slew rates and faster operation compared to conventional DAC chips, ensuring more precise signal generation.

The driving stage circuit is equally important, as it is responsible for delivering the required output currents to the target tissues. Constant current circuits are generally preferred for maintaining consistent stimulation, despite variations in tissue impedance [25]. Various designs have been proposed to enhance the efficiency of driving circuits, including H-bridge configurations and voltage-controlled current sources (VCCS), which offer improved operational efficiency and scalability for multi-channel applications [1–3,8–11,13,17,18,21]. This study integrates a constant current driving stage with H-bridge networks and feedback control, ensuring stable output currents across a wide range of therapeutic applications [25].

Addressing the need for versatile, locally accessible ES devices is crucial, particularly in regions like Thailand, where high costs and limited access to advanced medical tech-

nologies present significant challenges for smaller hospitals and clinics. While current research often focuses on portable or wearable ES devices, which prioritize miniaturization, cost-effectiveness, low power consumption, and personalization [15,18–20], the proposed stationary ES device remains equally important. There is still significant demand for stationary systems in clinical settings, where adaptability, high performance, and versatility are essential to meet a wide range of therapeutic needs. By utilizing in-house technology and locally sourced components, the proposed device not only reduces costs but also enhances accessibility, ensuring that healthcare providers in resource-limited areas can deliver comprehensive and effective treatments.

The key contributions of this work lie in the development of a multi-functional and cost-efficient ES device that addresses several limitations inherent in existing technologies. By incorporating high-resolution signal generation, flexible waveform patterns, and precise control, the proposed device significantly improves upon conventional systems. Additionally, the use of a discrete R-2R ladder DAC circuit and an advanced driving stage configuration ensures superior performance in generating non-linear signals necessary for various therapeutic applications. This research not only advances the field of electrical stimulation technology but also provides practical solutions for improving healthcare accessibility, particularly in regions with limited resources.

The scope of this study focuses on the design, implementation, and evaluation of the proposed multi-functional ES device. Emphasis is placed on the pulse generator and driving stage units, which are critical in ensuring the precision and effectiveness of the device's output signals. While this study primarily targets applications in physiotherapy, rehabilitation, and pain management, it also lays the groundwork for future innovations in the field of electrical stimulation. A comprehensive assessment of the device's capabilities, including its waveform generation, signal precision, and adaptability to various therapeutic needs, is conducted with the aim of enhancing the versatility of ES applications.

The structure of this paper is as follows: Section 1 presents the background and significance of the research, establishing the rationale and context for the development of the proposed electrical stimulation (ES) device. Section 2 provides a detailed account of the methodologies employed in the design and implementation of the system, with particular emphasis on the technical aspects of the pulse generator and driving stage. Section 3 describes the experimental setup, configurations, and results. Section 4 offers a comprehensive discussion of the findings. Finally, Section 5 concludes the paper by summarizing the key insights and contributions of the study.

2. Methodology

2.1. System Overview

This section provides an overview of the proposed 2-channel, multi-functional therapeutic ES device, as depicted in Figure 1. The system comprises four main units: (A) the user interface (UI) and controller unit, (B) the pulse generator unit, (C) the driving stage unit, and (D) the protection unit. Each unit plays a critical role in ensuring the device's functionality, reliability, and safety across diverse therapeutic applications.

(A) UI and Controller Unit

The UI has been designed to fulfill three primary functions: input peripheral, display, and system notification. There are five components in this UI design: a multipoint touchscreen, push-button switches, a rotary switch, LED indicators, and a buzzer. A multipoint touchscreen integrated with a rotary switch was designed to serve as the primary input peripheral in this sub-unit. However, additional physical push buttons may be employed according to user preferences or as a contingency in the event of a multipoint touchscreen malfunction. The display sub-unit was designed to present essential information, such as system configurations, parameter settings, operating time and status, notification status, system help, and the user manual. The notification sub-unit integrates LED indicators, an audible buzzer, and on-screen status alerts to notify users.

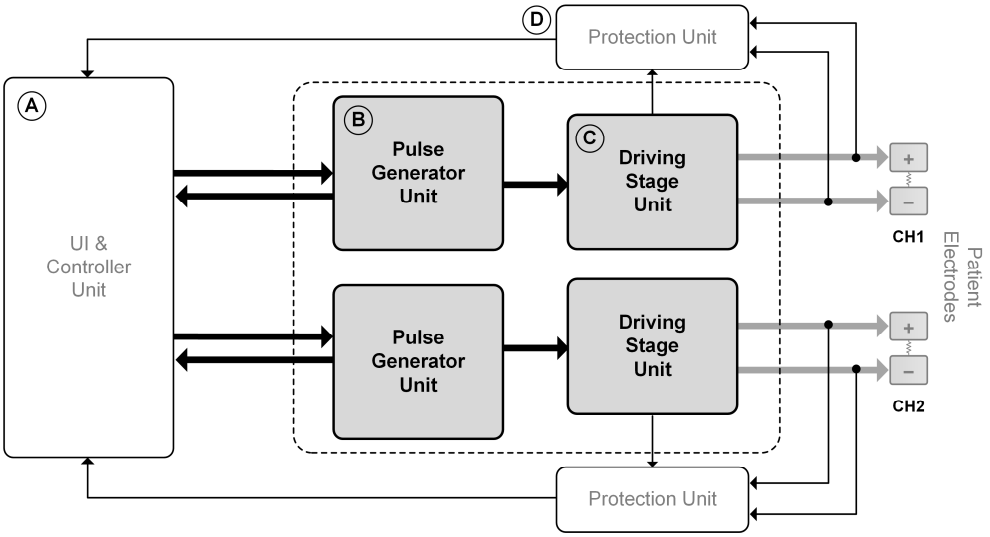

Figure 1. System overview of the proposed ES design.

The dsPIC33EP512MU810 microcontroller was selected as the core MCU and controller for this design, responsible for managing all operational functions and co-ordinating communication across three key units: the user interface (UI), the pulse generator, and the driving stage. This controller processes inputs from various sub-units, executes control algorithms, manages computations, accesses memory and storage, and interacts with peripheral devices. By overseeing the entire system's operation, the microcontroller ensures seamless communication between components and maintains the proper functioning of the system. Specifically, it plays a central role in interfacing with the UI, pulse generator, and system protection units, ensuring effective and reliable performance.

(B) Pulse Generator Unit

The unit is responsible for synthesizing pulses corresponding to parameters provided by (A). This unit must possess the capability to generate highly nonlinear waveforms at a high-resolution level, allowing for flexible adjustments of various pulse train amplitudes, durations, and frequencies. The specifications of this design must incorporate the twelve essential waveforms commonly used in physiotherapy, as identified through a preliminary survey of a large group of physiotherapists and rehabilitation doctors for effective treatment, as mentioned in [28].

These waveforms include IG, CG, MF, DF, CP, CPid, LP, TF, RF, ASYM, ASYM-A, and SYM. Additionally, two extra special functions have been incorporated. Each essential waveform allows for pulse amplitude adjustment within a range of 0–140 mA, pulse duration within ranges of 20–1,000,000 µs, and pulse repetitive frequency within a range of 0–1000 Hz. Furthermore, the two special functions enable modulation of the twelve essential waveforms using Surge and Modulation techniques, facilitating the generation of a wider variety of stimulation patterns.

(C) Driving Stage Unit

This unit has two primary functions: (1) amplifying the analog voltage signals from (B) to the necessary levels and (2) converting amplified voltage signals into current signals with identical shapes for delivery to the patient electrodes. By integrating these two key functions, the proposed driving stage unit, in conjunction with an H-bridge circuit, functions as a constant current source, ensuring precise voltage-to-current conversion and maintaining stable current outputs under varying load conditions.

(D) Protection Unit

The unit is responsible for ensuring the safety and well-being of patients or users. It monitors real-time input signals from the patient electrodes and sends to (A) for real-time

analysis and appropriate actions. It is designed to prevent potentially unsafe conditions during ES operation, which could occur due to various causes; for example, the detachment of electrodes during use, inadequate contact between electrodes and human skin, or other electrical circuit malfunctions/faults. This unit was designed such that if either overvoltage/overcurrent problems or electrical faults occur, the unit will transmit logic 0 to (A), resulting in stopping operation of the entire ES device to assure the patient safety.

This research paper will primarily concentrate on, and provide an in-depth analysis of, the (B) pulse generator unit and the (C) driving stage unit. Figure 2 illustrates the scope of work emphasized in this paper.

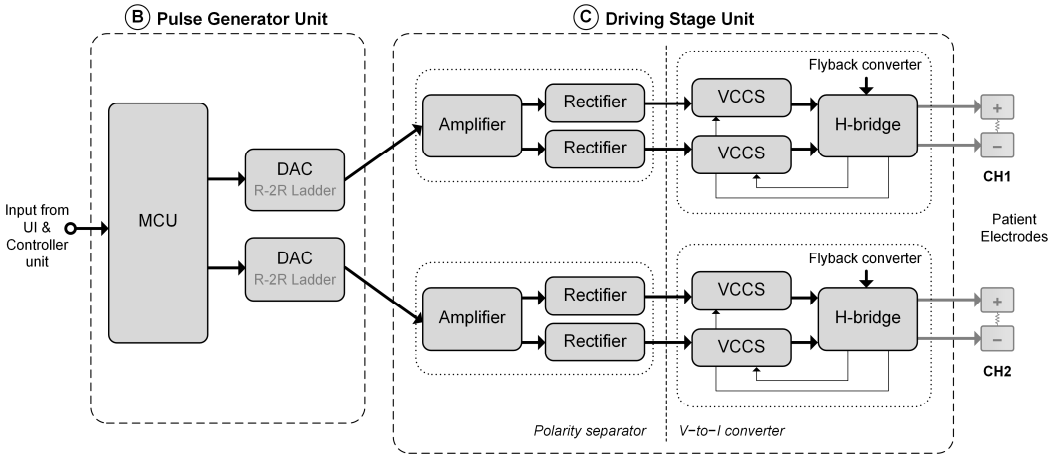

Figure 2. Scope of work emphasized in this paper.

2.2. Proposed Pulse Generator Unit

The pulse generator design in this research consists of two key components which includes the microcontroller (MCU) and the digital-to-analog converter (DAC).

2.2.1. MCU

This work applied a real-time technique in generating desired discrete digital signals. This design incorporates the dsPIC-33EP512MU810, a 16-bit DSP and high-speed microcontroller from Microchip Inc. (Chandler, AZ, USA). This MCU receives commands from the UI unit and generates discrete digital pulses corresponding to these commands. These digital pulses are mathematically computed and then transmitted directly to the DAC.

In this study, we utilized our proprietary in-house algorithms to generate the required waveforms. These algorithms are based on creating four fundamental signal types: direct current (DC) signal, sinusoidal signal, square wave, and triangular wave. By combining these four algorithms, our approach effectively generates and covers all twelve essential waveforms specified by our proposed multi-functional ES design, along with the two special functions previously mentioned. This method offers significant advantages over the traditional Look-Up Table (LUT) algorithm [1,2,4,7]. It is computationally inexpensive, faster, and requires fewer resources, thus enhancing speed, efficiency, and performance.

2.2.2. DAC

In this work, an R-2R ladder circuit, consisting of resistors with values of either R or 2R, was selected as the DAC. This choice meets the design requirements for resolution, speed, continuity, and notably higher slew rates compared to conventional DAC chips [29]. The proposed R-2R ladder DAC was paired with a high-speed operational amplifier (Op-Amp) to generate analog output signals, $V_{Ra}(t)$.

This design achieves a very high slew rate of 350 V/µs, and a bandwidth of 50 MHz [30], which is sufficient for generating highly non-linear signals with minimal distortion. Figure 3 illustrates the proposed R-2R ladder DAC developed in this work. Another advantage of employing an R-2R ladder circuit is its ability to interface with the MCU using

a parallel peripheral interface (PPI) via the MCU's input/output ports. This interface offers significantly faster communication speeds compared to the Serial Peripheral Interface (SPI) typically used in most of the DAC chips [31]. The enhanced speed provided by the PPI used in this work ensures more efficient data transmission, which is crucial for high-speed applications and complex waveform generation in therapeutic ES devices.

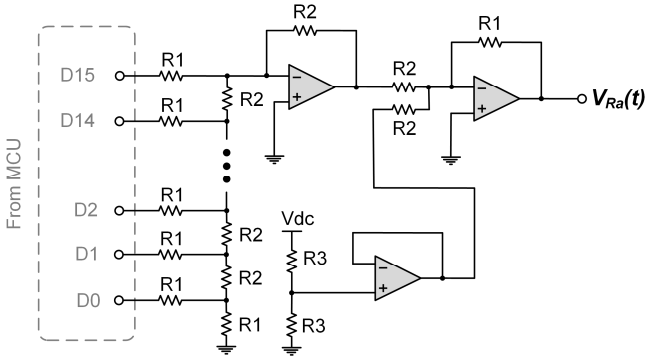

Figure 3. The proposed R-2R ladder DAC circuit.

The actual schematic of the proposed pulse generator unit implementation is depicted in Figure 4.

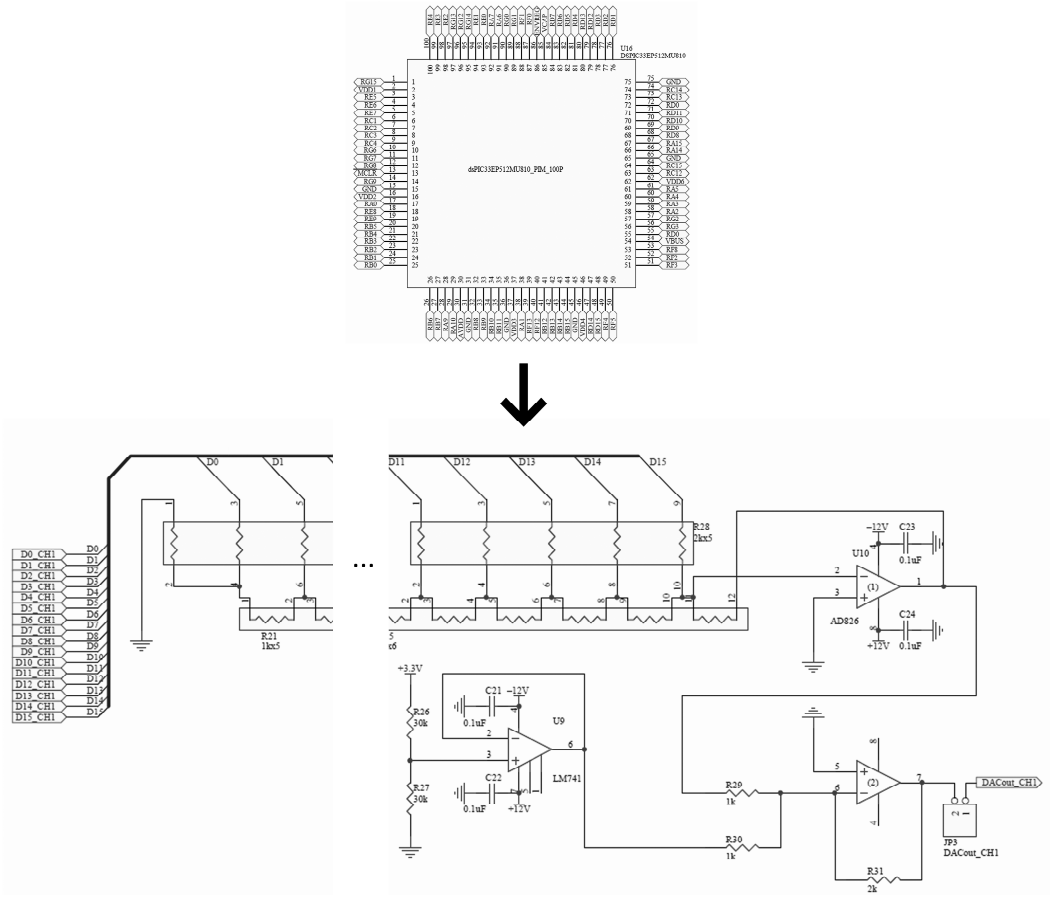

Figure 4. The actual schematic of the proposed pulse generator unit implementation.

2.3. Proposed Driving Stage Unit

The driving stage unit, commonly referred to as the ES power or ES output circuit, is primarily responsible for delivering the appropriately transformed current pulses to the targeted patient tissues, ensuring the intensity settings prescribed by the physiotherapist

are met. This unit comprises two essential components: (1) the polarity separator and (2) the voltage-to-current (V-to-I) converter, as depicted in Figure 2.

2.3.1. Polarity Separator

The polarity separator, shown in Figure 2, generates control signals for the Voltage-Controlled Current Source (VCCS) and H-bridge circuit within the V-to-I converter. This separator utilizes an inverting amplifier and two half-wave rectifier circuits, as depicted in Figure 5, to decompose any analog input voltage, $V_{Ra}(t)$, from the previous DAC into its positive and negative components, $V_{Ra}+(t)$ and $V_{Ra}-(t)$. These decomposed signals are then sent to the V-to-I converter for further processing.

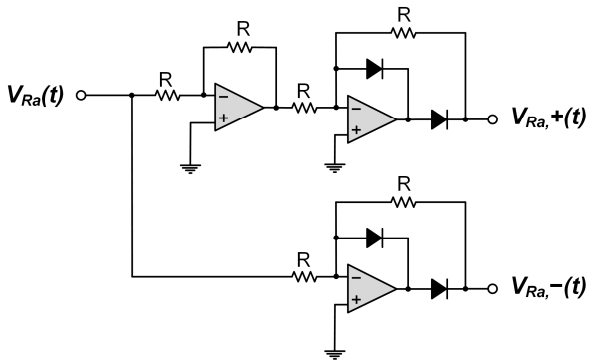

Figure 5. The signal polarity separator circuit in this design.

2.3.2. V-to-I Converter

The V-to-I converter in this study was designed using two VCCS circuits in conjunction with an H-bridge circuit, as illustrated in Figure 6. The VCCS circuits are essential for controlling the pulse shapes, amplitudes, and polarities of the desired output currents. The H-bridge circuit, which contains four transistors (Q1, Q2, Q3, and Q4), operates in pairs and is controlled by the two VCCS circuits. The right-hand VCCS circuit, consisting of U1 and Q5, controls transistors Q1 and Q2 to produce a positive-directional current flow. Conversely, the left-hand VCCS circuit, consisting of U2 and Q6, controls transistors Q3 and Q4 to produce a negative-directional current flow.

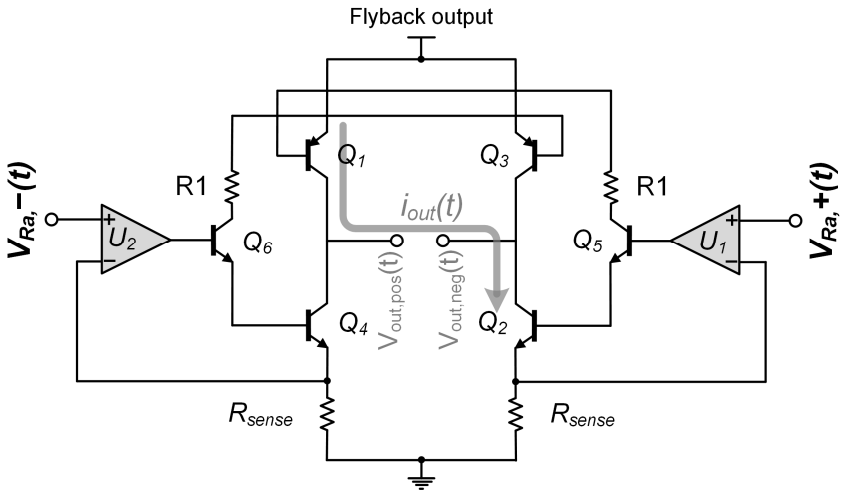

Figure 6. V-to-I converter in this work.

The H-bridge circuit outputs for each channel are directly connected to two electrodes, which attach to the patient's skin or targeted tissues. Two feedback signals from *R-sense* resistors in the H-bridge outputs, along with the two polarized output signals from the DAC, are simultaneously compared and adjusted to maintain a constant current output

as set by the users. This ensures accurate and consistent delivery of therapeutic output currents [25]. The proposed driving stage unit, as in Figure 6, is designed to generate a maximum output current of 150 mA on both the negative and positive sides. The output characteristics of this driving stage unit can be derived by the following equation:

$$i_{out}(t) = \frac{V_{out,pos}(t)}{R_{sense}} + \frac{V_{out,neg}(t)}{R_{sense}} \quad (1)$$

The flyback converter in Figure 6 is integrated as the power supply for the H-bridge circuit. Given the direct interface of the H-bridge with human skin, ensuring safety is paramount. To this end, an isolated flyback converter, depicted in Figure 7, has been utilized for its robust safety features. This converter produces an output voltage of 150 volts and can deliver a maximum current of 200 mA. Safety is ensured through the use of a transformer with a 13:115 turns ratio. The flyback circuit is regulated by the TL494 IC, operating at a switching frequency of 50 kHz, and employs a constant voltage with pulse width modulation (PWM) controller. This configuration ensures stable and reliable power delivery while maintaining stringent safety standards [32].

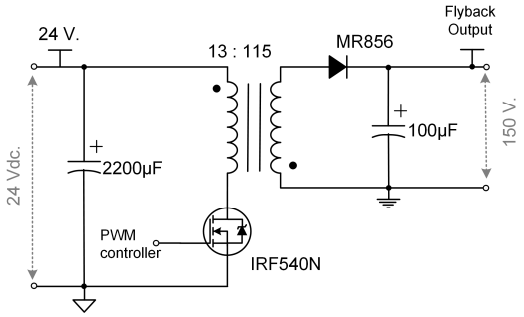

Figure 7. The flyback converter circuit.

The actual schematic of the proposed driving stage unit implementation is depicted in Figure 8. This figure provides a detailed illustration of the circuitry and components involved in achieving the desired voltage-to-current conversion.

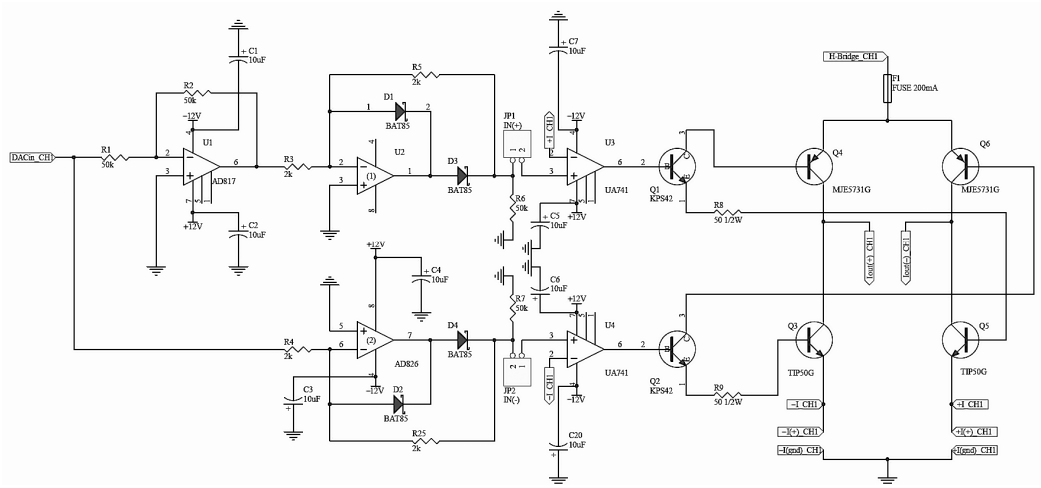

Figure 8. The actual schematic of the proposed driving stage unit implementation.

2.4. Proposed Target Outputs: Essential Waveforms and Special Functions

In this section, we provide a brief definition and description of the essential waveforms and special functions that form the foundation of the proposed ES device. These target outputs were carefully selected based on the recommendations and requests gathered from a preliminary survey of a large group of local physiotherapists and rehabilitation doctors.

Their input has shaped the design to ensure that the device meets the practical needs of therapeutic applications. Specifically, the twelve essential waveforms identified in the survey will serve as mandatory output options for this device.

A key advantage of our design, which leverages in-house technology, proprietary algorithms, and a versatile hardware configuration, is its flexibility for future expansion. Should additional therapeutic waveforms or specialized output current requirements arise, the system can be easily modified to accommodate more than the initial twelve waveforms. Furthermore, the adjustability of both existing and future waveforms can be expanded as needed, ensuring that the design remains adaptable to evolving clinical demands.

2.4.1. Twelves Essential Waveforms [22,27,28,33,34]

(1) Interrupted Galvanic (IG) Waveform: The IG waveform is a direct current (DC) that is periodically interrupted, producing a series of short pulses. This waveform is particularly beneficial for deep tissue stimulation and is effective in inducing muscle contractions. It is commonly used for rehabilitating paralyzed muscles and improving blood circulation, making it ideal for patients with muscle atrophy or peripheral nerve injuries. The IG waveform promotes better muscle tone and enhances tissue oxygenation, which aids in recovery and rehabilitation.

(2) Continuous Galvanic (CG) Waveform: The CG waveform consists of a continuous, unmodulated direct current (DC). It is primarily used for pain relief in chronic conditions such as arthritis and inflammatory diseases. The continuous nature of the CG waveform helps reduce inflammation, and it is also utilized in iontophoresis treatments, where it facilitates the delivery of medications into tissues. This targeted approach provides localized therapeutic effects, making CG an effective solution for patients requiring pain management and anti-inflammatory therapy.

(3) Monophase Fixed (MF) Waveform: The MF waveform is a single-phase, rectified sinusoidal current with a frequency of 50 Hz. Its consistent, unidirectional current reduces skin resistance, allowing deeper tissue penetration. This makes the MF waveform especially useful for pain relief in deep muscles and muscle strengthening. It is frequently employed in the treatment of patients with muscle weakness or those recovering from injury, as it delivers targeted stimulation to the affected muscle groups.

(4) Diphase Fixed (DF) Waveform: The DF waveform features a dual-phase, rectified sinusoidal current with a frequency of 100 Hz. By alternating between positive and negative phases, the DF waveform ensures balanced muscle stimulation. It is highly effective for pain relief, improving circulation, and treating muscle spasms. This waveform is particularly useful in post-operative recovery, as it reduces pain while promoting faster muscle recovery and rehabilitation.

(5) Courted Period (CP) Waveform: The CP waveform alternates rapidly between one second of Monophase Fixed (MF) current and one second of Diphase Fixed (DF) current. This alternating current is highly effective for muscle re-education and strengthening, as it generates consistent muscle contractions without causing discomfort. The CP waveform is particularly beneficial for patients recovering from stroke or neurological injuries, as it supports muscle recovery without excessive fatigue.

(6) Courted Period Iso-Dynamic (CPid) Waveform: Similar to the CP waveform, the CPid waveform alternates between MF and DF currents, but with the MF phase having 12.5% lower amplitude than the DF phase. This configuration helps to prevent muscle fatigue while providing intermittent muscle contractions, making the CPid waveform ideal for muscle strengthening and functional rehabilitation. It is commonly used in neuromuscular training, where controlled and alternating stimulation is required for effective recovery.

(7) Long Period (LP) Waveform: The LP waveform alternates between six seconds of Monophase Fixed (MF) current and six seconds of Diphase Fixed (DF) current. During the DF phase, additional pulses with gradually increasing and decreasing amplitude

are introduced. This gradual modulation makes the LP waveform particularly useful for activating larger muscle groups, such as those in the legs and back. It is highly beneficial for lower limb rehabilitation, posture correction, and spinal cord injury recovery, as it provides deeper and more sustained stimulation.

(8) Triangular Faradic (TF) Waveform: The TF waveform is a saw-tooth shaped current with adjustable parameters for amplitude, duration, and frequency. Its gradual rise and fall pattern provides a smooth stimulation, which is particularly effective for muscle re-education and tissue healing. This waveform is ideal for patients recovering from injury or surgery, where muscle strength needs to be regained gradually and progressively.

(9) Rectangular Faradic (RF) Waveform: The RF waveform is a rectangular-shaped pulsed current with adjustable settings for amplitude, duration, and frequency. It is commonly used for targeted muscle stimulation and nerve activation, particularly in Functional Electrical Stimulation (FES). The RF waveform helps restore movement in patients with neurological disorders such as stroke or multiple sclerosis by delivering precise, controlled stimulation to specific muscle groups.

(10) Asymmetrical (ASYM) Waveform: The ASYM waveform is a monophasic, asymmetrical pulsed current. It is particularly effective for preventing muscle fatigue and improving endurance during long-term therapy. The asymmetrical pulse reduces skin irritation, making it suitable for patients who require chronic pain management or muscle rehabilitation over extended periods. Its gentle, continuous stimulation helps sustain therapy without causing discomfort.

(11) Asymmetrical Alternating (ASYM-A) Waveform: The ASYM-A waveform is a biphasic, asymmetrical pulsed current that provides greater control over the intensity of stimulation. This waveform is beneficial for gradual muscle strengthening and preventing muscle atrophy. It is particularly effective in progressive rehabilitation programs, as clinicians can adjust the intensity and balance of the pulses as the patient's muscle strength improves over time.

(12) Symmetrical (SYM) Waveform: The SYM waveform is a biphasic, symmetrical pulsed current that ensures equal stimulation across muscle groups. This balanced stimulation reduces the risk of muscle fatigue and tissue irritation, making it ideal for muscle reconditioning. The SYM waveform is commonly used in bilateral limb rehabilitation, where balanced muscle development on both sides of the body is crucial for recovery and overall functionality.

2.4.2. Two Special Functions [33–35]

The following section explains the two special functions, Surge and Modulation, emphasizing their necessity and the contributions they bring to standard therapeutic protocols. These functions are designed to enhance conventional therapy by offering more controlled and dynamic stimulation options, improving both the flexibility and efficacy of treatment.

(1) Surge provides a gradual increase and decrease in intensity, allowing for deeper tissue targeting while minimizing abrupt changes in stimulation. This function is particularly beneficial for pain management and muscle stimulation, offering patients a smoother and more comfortable therapeutic experience.

(2) Modulation introduces variations in the frequency or intensity of the current, preventing the body from adapting or habituating to the therapy. By maintaining the body's response to stimulation over extended periods, Modulation enhances the effectiveness of long-term treatments.

In comparison to standard therapy, the integration of Surge and Modulation offers greater flexibility and adaptability, enhancing patient comfort and potentially leading to better therapeutic outcomes. These functions are especially valuable in personalized treatments, where static waveforms may be less effective. Electrical stimulation devices

without these features may still provide effective therapy but are often limited in terms of comfort, adaptability, and long-term efficacy.

2.5. Design Specifications and Operational Ranges of the Proposed ES Device

Table 1 below presents the design specifications of the proposed ES device, offering a comprehensive overview of its capabilities. It highlights the intricate relationship between the device's adjustable parameters and their respective operational ranges. Given the device's twelve essential output current patterns, understanding these interactions is crucial for optimizing its performance. The table is structured to clarify how each parameter can be tuned within its specific limits, offering a detailed matrix that captures the nuanced relationships between the various output patterns and their respective adjustable ranges. This organized approach shown in Table 1 will help readers navigate the complexities of the proposed ES device's specifications and its operational ranges with greater ease and precision.

Table 1. Design specifications and operational ranges of the proposed es device.

Output Current Patterns		Group	Operational Ranges and Its Adjustability			Special Functions Availability	
			Pulse Amplitude (mA)	Pulse Duration (μs)	Pulse Repetitive Frequency (Hz)	Surge	Modulation
1	IG	Galvanic	0–40	-	-	-	-
2	CG		0–40	-	-	-	-
3	MF	Diadynamic	0–70	-	-	Yes	-
4	DF		0–70	-	-	Yes	-
5	CP		0–70	-	-	-	-
6	CPid		0–70	-	-	-	-
7	LP		0–70	-	-	-	-
8	TF	Faradic	0–80	20–1,000,000	0.2–1000	Yes	Yes
9	RF		0–80	20–1,000,000	0.2–1000	Yes	Yes
10	ASYM	TENS	0–140	20–400	1–200	Yes	Yes
11	ASYM-A		0–140	20–400	1–200	Yes	Yes
12	SYM		0–140	20–400	1–200	Yes	Yes

2.6. Implementation

Each component mentioned in Sections 2.2 and 2.3 has undergone extensive testing to ensure its functionality. The circuits and printed circuit board (PCB) designs were deliberately optimized for a wide range of scenarios, ensuring reliability across various essential waveforms and the two special functions. Eventually, all the components were integrated into two PCBs, each dedicated to its specific functions, as shown in Figure 9.

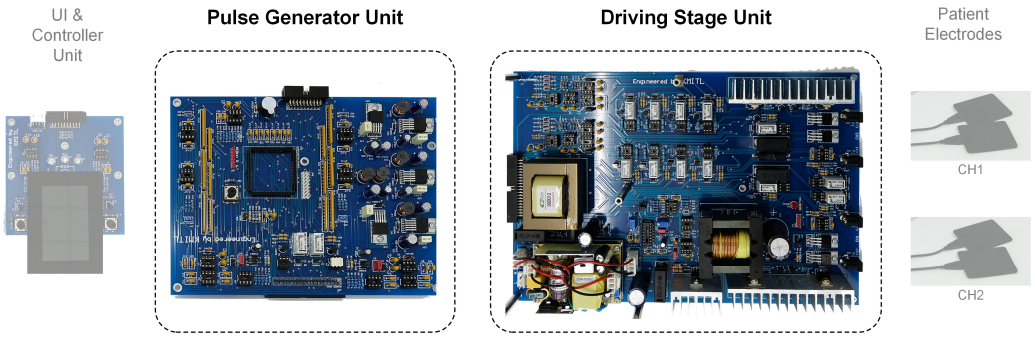

Figure 9. Two integrated PCBs of the key components in the proposed ES design.

3. Experiments and Results

This section presents the experimental evaluation of the proposed ES device. The experiments were designed to assess the device's performance across various critical dimensions, including its ability to generate diverse therapeutic waveforms, maintain precise and stable output currents, and adhere to stringent international standards for medical electrical equipment. The experimental setup was carefully configured to imitate several clinical conditions, ensuring that the experimental results obtained are meaningful and applicable to practical therapeutic treatment scenarios [6,26]. The following sections provide a comprehensive assessment of the device's performance and reliability covering test configurations, output demonstration and accuracy, stability under variable load conditions, and compliance with the relevant IEC standards.

3.1. Test Configurations

The experimental setup, as illustrated in Figure 10, was meticulously configured to evaluate the performance of the proposed ES device across various tests. Figure 11 illustrates the actual experimental setup including all equipment used. The process began with the pulse generator unit, which received input configuration settings from the UI and controller unit. These settings were processed to generate voltage pulse signals, denoted as V_{Ra}, which were subsequently fed into the driving stage unit. The driving stage unit converted these voltage pulse signals into output currents I_{Out}, which were then delivered directly to a resistive load R, simulating the impedance of human tissue [1].

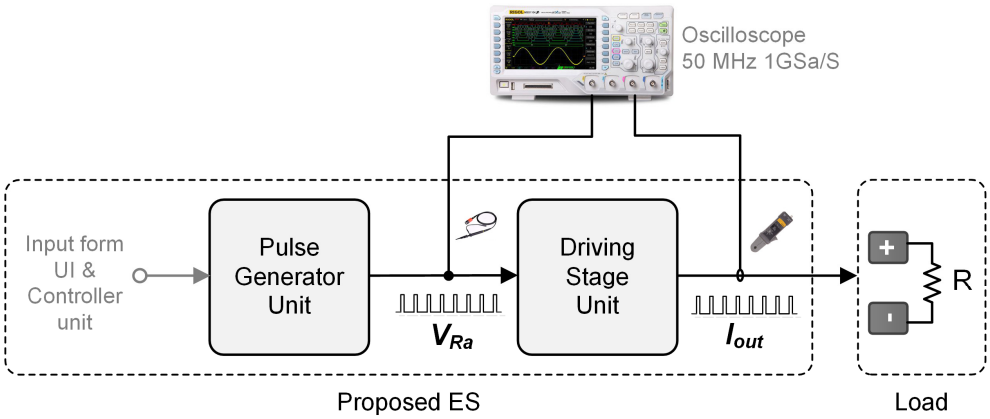

Figure 10. The experimental configuration diagram.

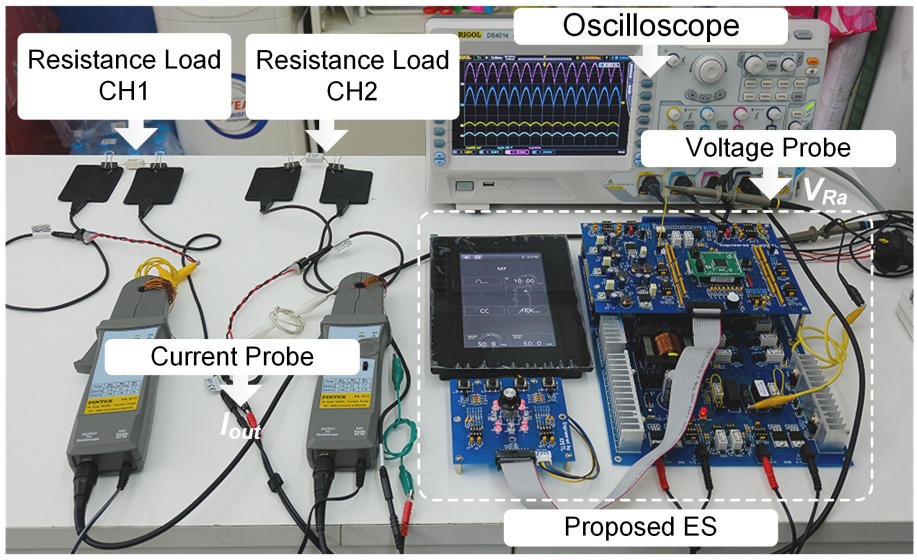

Figure 11. The actual experimental setup.

To monitor and record the waveforms of both V_{Ra} and I_{Out}, a high-precision 50 MHz, 1 GSa/s oscilloscope was employed. Channel 1 of the oscilloscope was equipped with a 150 MHz voltage probe, specifically to monitor the voltage signal V_{Ra} (t) in real time. Meanwhile, Channel 2 was connected to a high-precision current probe with a bandwidth ranging from DC to 50 MHz, enabling accurate measurement of the output current $I_{Out}(t)$ also in real time. The oscilloscope captured these signals both graphically and as raw data in comma-separated value (CSV) format for further analysis. This setup ensured that both the voltage and current waveforms were captured with high fidelity, facilitating a detailed and precise analysis of the device's performance.

3.2. Demonstration of Proposed ES Output Currents: Essential Waveforms, Adjustability, and Special Functions

The main objective for this test was to demonstrate and evaluate capabilities of the proposed ES device in generating all twelve essential therapeutic output currents, including its adjustability and also two special functions (Surge and Modulation).

3.2.1. Essential Waveforms Demonstration

Figure 12 presents the experimental results where the proposed ES device was configured to deliver a constant 40 mA across each of the twelve essential current outputs (IG, CG, MF, DF, CP, CPid, LP, TF, RF, ASYM, ASYM-A, and SYM). The voltage signal, V_{Ra}, generated by the pulse generator unit, and the corresponding output currents, I_{Out}, produced by the driving stage unit, were captured via Channel 1 (blue) and Channel 2 (red) of the oscilloscope, respectively.

The results across all twelve sub-figures confirm the close alignment between V_{Ra} and I_{Out} waveforms, with consistent similarities in shape, pulse duration, and pulse repetitive frequency. Additionally, the current output amplitudes are precisely aligned with the gain, as can be derived from Equation (1).

It is important to note that Figure 12 provides examples of each essential current output waveform. Given the wide range and variability of output adjustability, it is not feasible to display every possible variation of the twelve waveforms.

3.2.2. Adjustability Demonstration

The experimental results presented in Figures 13–15 highlight the performance of the proposed ES device across three main adjustable parameters, including pulse amplitude, pulse duration, and pulse repetitive frequency. These figures demonstrate the proposed ES device's ability to be precisely configured to achieve the target outputs for each parameter.

In Figure 13, the MF current pattern was selected as a representative of sinusoidal-based current signals, while the ASYM current pattern was chosen as a representative of pulse-based current signals to illustrate the pulse amplitude adjustability of the proposed ES device. The target of output current amplitude was set at approximately 10%, 50%, and 100% of the rated output current for each pattern, with pulse duration and pulse repetitive frequency held constant. The experimental results confirm that the proposed ES device accurately generates the pulse amplitude as set for both sinusoidal-based and pulse-based output currents, with minimal to zero distortion in waveform shape, pulse duration, and pulse repetitive frequency.

In Figure 14, only the ASYM current pattern is used to demonstrate and validate the pulse duration adjustability of the proposed ES device. The sinusoidal-based current patterns were considered necessary only for amplitude adjustability, in alignment with actual clinical practice and the requirements of doctors and physiotherapists [22]. Pulse duration adjustability was tested and recorded at 50 μs, 500 μs, and 2000 μs, with pulse amplitude and pulse repetitive frequency held constant. The experimental results confirm that pulse duration can be accurately adjusted and configured to meet a wide range of clinical needs.

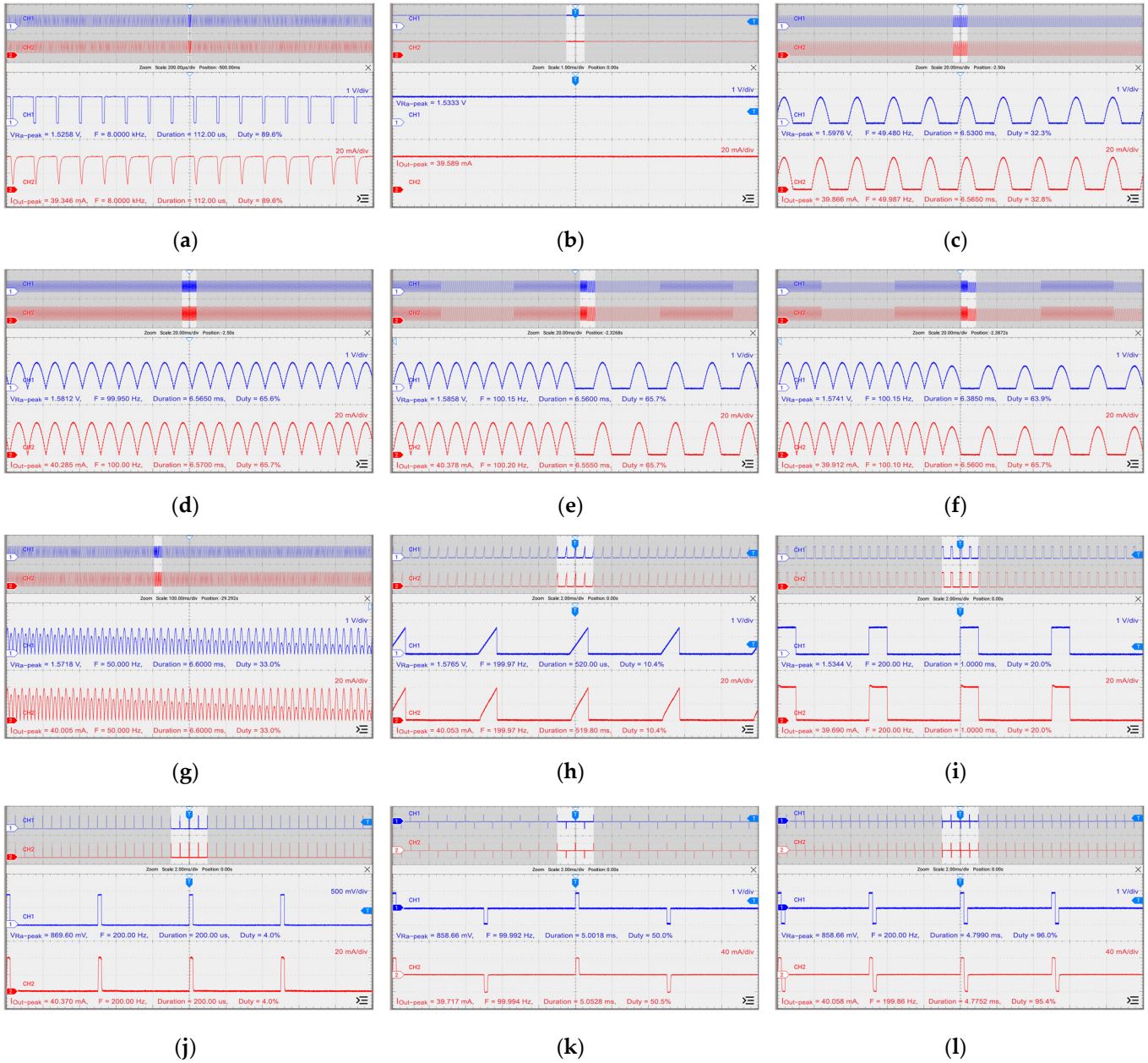

Figure 12. Demonstration of twelve essential output currents (I_{Out}) compared to controlled voltage (V_{Ra}) of the proposed ES device: (**a**) IG; (**b**) CG; (**c**) MF; (**d**) DF; (**e**) CP; (**f**) CPid; (**g**) LP; (**h**) TF; (**i**) RF; (**j**) ASYM; (**k**) ASYM-A; and (**l**) SYM.

Figure 15 illustrates the experimental results for pulse repetitive frequency adjustability, using the RF current pattern as a representative at 50 Hz, 200 Hz, and 500 Hz. The experimental results verify that pulse repetitive frequency can be adjusted precisely without affecting the pulse amplitude or pulse duration, both of which were held constant.

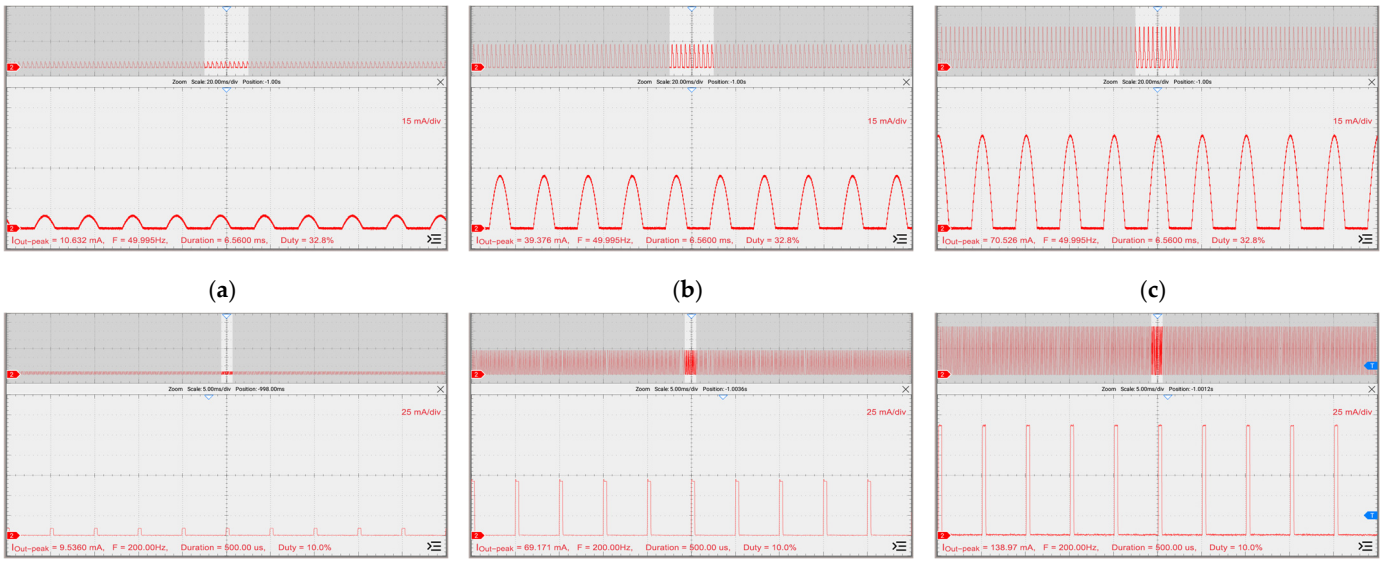

Figure 13. Demonstration of pulse amplitude adjustability: (**a**) MF 10 mA; (**b**) MF 40 mA; (**c**) MF 70 mA; (**d**) ASYM 10 mA; (**e**) ASYM 70 mA; and (**f**) ASYM 140 mA.

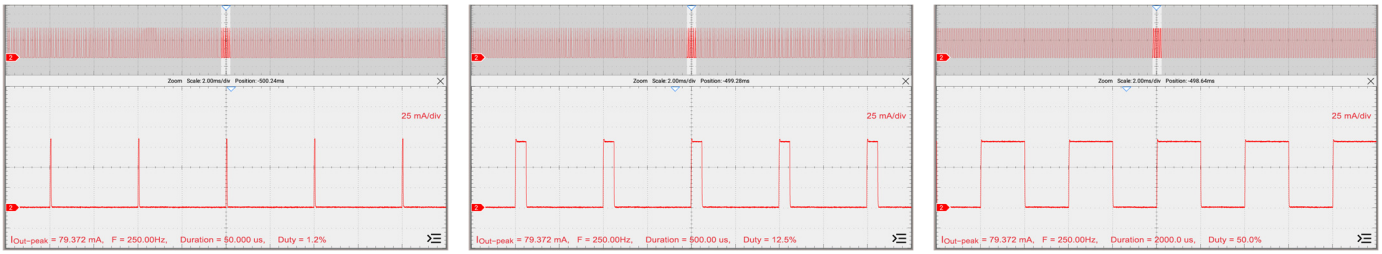

Figure 14. Demonstration of pulse duration adjustability (ASYM): (**a**) 50 µs; (**b**) 500 µs; and (**c**) 2000 µs.

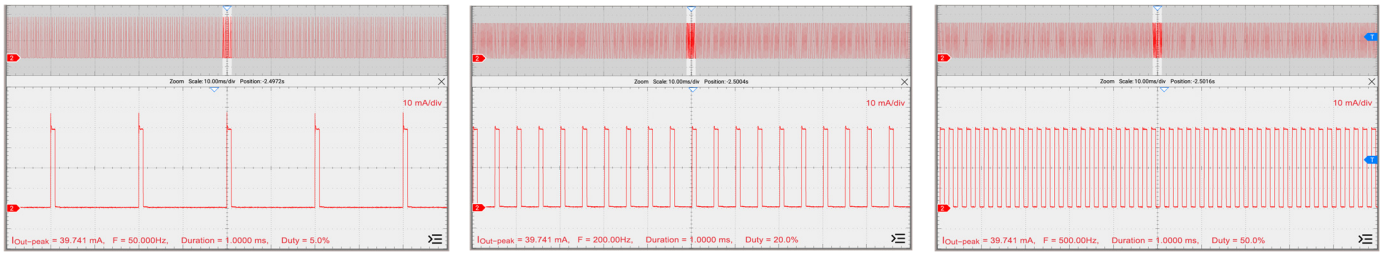

Figure 15. Demonstration of pulse repetitive frequency adjustability (RF): (**a**) 50 Hz; (**b**) 200 Hz; and (**c**) 500 Hz.

3.2.3. Special Functions Demonstration

This experiment was conducted extensively across various modulated settings to ensure precise alignment and reliability in modulating each of the twelve essential output patterns using two special functions: Surge and Modulation. Figure 16 presents example results for some of these essential output waveform modulations achieved with the Surge and Modulation techniques.

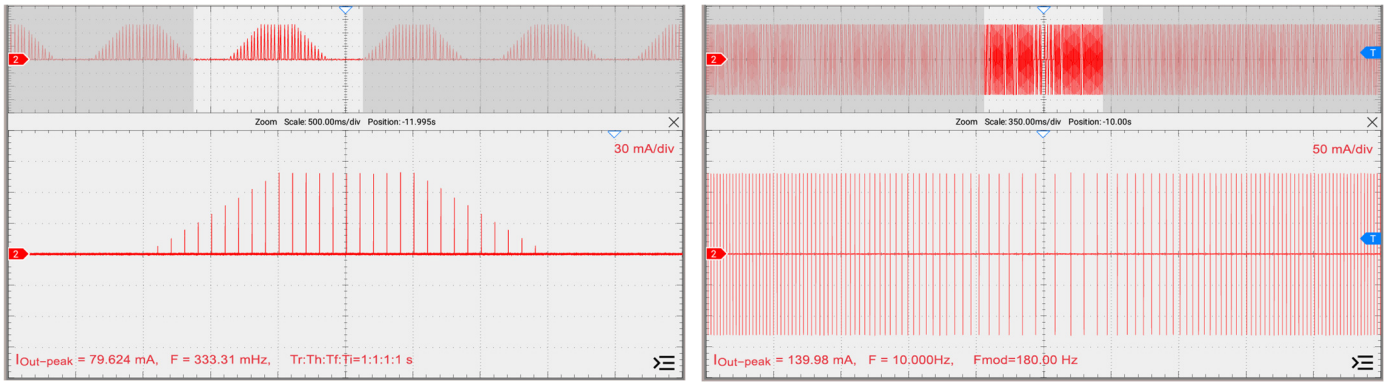

(**a**) (**b**)

Figure 16. Demonstration of two additional special functions for output currents.: (**a**) ASYM with Surge; and (**b**) SYM with Modulation.

3.3. Output Accuracy Verification Test in Compliance with IEC Standards

The experimental setup adhered to the guidelines outlined in Clause 201.12.1.102 of the IEC 60601-2-10 standard [36], which addresses the basic safety and essential performance requirements for nerve and muscle stimulators, specifically concerning pulse parameter accuracy control. The standard emphasizes that the accuracy of current outputs is critical for ensuring the safety and effectiveness of therapeutic applications. It specifies that pulse durations, pulse repetitive frequencies, and pulse amplitudes—including any DC components caused by offsets or asymmetrical waveforms—must not deviate by more than ±20% when measured with a specified load resistance. This tolerance is established to ensure that the proposed ES device functions within safe and effective parameters, thereby minimizing the risks associated with significant deviations in stimulation characteristics. The primary objective of this test was to verify that the proposed ES device consistently delivers the intended therapeutic output current across a range of test conditions and settings.

The testing procedure was conducted in three configurations: pulse amplitude test, pulse duration test, and pulse repetitive frequency test. Each stage focused on isolating a specific parameter while maintaining the other two parameters constant. Testing was performed across the entire operational range of each output current pattern, divided into ten incremental steps from the minimum to the maximum values within each range, using the specific load resistance specified in the standard. At each step, the output was measured, and the deviation percentage between the setting value and the measured value was calculated.

To evaluate the accuracy of the proposed method's output current in relation to the reference tolerance specified in the IEC 60601-2-10 standard, the percentage of deviation (similar to percentage of error) is a valuable metric [37,38]. It helps quantify the difference between the output current and the reference value, providing a clear indication of how well the method adheres to the standard's tolerance requirements.

The percentage of deviation can be calculated as:

$$Percentage\ Deviation = \left(\frac{Measured\ value - Reference\ value}{Reference\ value} \right) \times 100 \quad (2)$$

where in this context, the Measured value refers to the output values of amplitude, duration, or frequency from the proposed device, while the Reference value refers to the setting value for each corresponding parameter.

This calculation provides a percentage that indicates how much the output current deviates from the acceptable tolerance defined by the standard. Lower percentage deviations indicate closer adherence to the reference tolerance, ensuring compliance with the standard's requirements.

To assess the consistency of the percentage deviations computed from each current output pattern for a sample size of ten (with ten incremental steps from the minimum to the maximum setting value), standard deviation (SD) serves as a valuable statistical measure [37,38]. SD quantifies the variation or dispersion of data points from the mean, providing insight into how closely the percentage deviations are clustered around the average value.

The standard deviation (SD) can be calculated as:

$$\mathrm{SD} = \sqrt{\frac{1}{N}\sum_{i=1}^{N}(x_i - \overline{x})^2} \tag{3}$$

where N is the number of samples (in this case, 10), x_i is each individual percentage deviation, and $\overline{x}$ is the mean of the percentage deviations.

A lower standard deviation indicates that the percentage deviations for the output current patterns are minimal, meaning that the data points are closely clustered around the mean. This suggests that the output currents are highly consistent and reliable across the ten samples for each pattern, as shown in Tables 2–4.

Table 2. Deviation and compliance with IEC standards in pulse amplitude variations.

Output Current Patterns		Pulse Amplitude Setting Range [22,39,40] (mA)	Percentage Deviation from 10-Step Increments of the Proposed Output Current (%)			IEC 60601-2-10 Maximum Deviation [36] (%)	Compliance [41–43]
			Min–Max	SD	Avg		
1	IG	0–40	2.05–6.00	1.17	3.49	20.00	Complied
2	CG	0–40	1.75–5.55	1.19	3.23	20.00	Complied
3	MF	0–70	0.13–3.93	1.39	1.01	20.00	Complied
4	DF	0–70	0.04–1.93	0.63	0.97	20.00	Complied
5	CP	0–70	0.27–4.00	1.39	1.05	20.00	Complied
6	CPid	0–70	0.23–4.00	1.17	1.23	20.00	Complied
7	LP	0–70	0.04–3.32	1.14	1.25	20.00	Complied
8	TF	0–80	0.13–1.31	0.44	0.60	20.00	Complied
9	RF	0–80	0.96–4.75	1.18	1.31	20.00	Complied
10	ASYM	0–140	1.62–8.14	1.70	4.33	20.00	Complied
11	ASYM-A	0–140	1.46–7.07	1.47	3.89	20.00	Complied
12	SYM	0–140	1.80–7.79	1.64	4.07	20.00	Complied

Table 3. Deviation and compliance with IEC standards in pulse duration variations.

Output Current Patterns		Pulse Duration Setting Range [22,39,40] (µs)	Percentage Deviation from 10-Step Increments of the Proposed Output Current (%)			IEC 60601-2-10 Maximum Deviation [36] (%)	Compliance [41–43]
			Min–Max	SD	Avg		
1	TF	20–1,000,000	0.00–0.50	0.15	0.07	20.00	Complied
2	RF	20–1,000,000	0.00–0.50	0.15	0.07	20.00	Complied
3	ASYM	20–400	0.00–1.25	0.46	0.39	20.00	Complied
4	ASYM-A	20–400	0.00–1.12	0.38	0.32	20.00	Complied
5	SYM	20–400	0.00–1.05	0.42	0.37	20.00	Complied

Table 4. Deviation and compliance with IEC standards in pulse repetitive frequency variations.

	Output Current Patterns	Pulse Repetitive Frequency Setting Range [22,39,40] (Hz)	Percentage Deviation from 10-Step Increments of the Proposed Output Current (%)			IEC 60601-2-10 Maximum Deviation [36] (%)	Compliance [41–43]
			Min–Max	SD	Avg		
1	TF	0.2–1000	0.00–0.30	0.09	0.04	20.00	Complied
2	RF	0.2–1000	0.00–0.30	0.09	0.04	20.00	Complied
3	ASYM	1–200	0.00–0.17	0.05	0.04	20.00	Complied
4	ASYM-A	1–200	0.00–0.14	0.05	0.03	20.00	Complied
5	SYM	1–200	0.00–0.14	0.05	0.03	20.00	Complied

In this context, a small SD reflects well on the performance of the proposed method, as it demonstrates that the variations between the measured output currents and the reference tolerance are minimal, implying good accuracy and stability across different output patterns.

The experimental results, presented in Tables 2–4, illustrate the deviations observed when varying pulse amplitudes, pulse durations, and pulse repetitive frequencies across all twelve essential output current patterns, respectively. These tables detail the percentage deviations for each parameter, including the minimum value, maximum value, average value, and standard deviation (SD) of the percentage deviations observed as the parameter settings of each pattern were varied.

Table 2 presents the percentage deviation in pulse amplitude, which was observed to be within the range of 0.04% to 8.14%, remaining well below the maximum allowable limit specified by the IEC standard. Additionally, the SD of the percentage deviation ranged from 0.44% to 1.70%, indicating a high level of consistency in generating outputs across different pulse amplitude levels.

Table 3 illustrates the percentage deviation in pulse duration, which was minimal, ranging from 0.00% to 1.25%, and remained within the IEC maximum allowable limit. The SD of the percentage deviation ranged from 0.15% to 0.46%, reflecting the system's consistency in generating the desired output currents across various pulse duration levels.

Table 4 shows the percentage deviation in pulse repetitive frequency, which was exceptionally low, ranging from 0.00% to 0.30%, again well within the IEC maximum allowable limit. The SD of the percentage deviation was below 0.1%, demonstrating the system's consistent performance across different pulse repetitive frequency levels.

It should be noted that the experimental results presented in Tables 3 and 4 do not include all twelve output current patterns. Instead, they only emphasize the current patterns that are most commonly adjusted by physiotherapists and therapeutic doctors, based the preliminary survey mentioned before. The remaining patterns are also capable of pulse duration adjustment if desired.

One conclusion can be drawn from Tables 2–4 is that the proposed device demonstrates exceptionally high accuracy in generating various output currents, regardless of variations in pulse amplitude, pulse duration, and pulse repetitive frequency. This is evident when comparing the results with the compliance requirements of the IEC standard. The deviations outlined in the standard have been adhered to and met efficiently. Additionally, a low percentage of SDs observed indicate the reliability of the output currents generated by the proposed ES device. This confirms the device's performance in achieving precise, predictable, and efficient output currents.

3.4. Stability Analysis of Constant Current Output

The stability of constant current output is a crucial factor in the reliable delivery of therapeutic currents to real-world patients, ensuring that the proposed ES device performs effectively without fluctuations, even when faced with changes in load resistance. This test

aimed to evaluate the reliability of the proposed ES device in maintaining consistent and constant output currents under varying load conditions, which simulate the diversity and variability of patient-specific impedance during treatment.

The testing procedure involved setting the target output current at the maximum value of each current range limit, according to the individual output current patterns shown in 5. The output current amplitude of the proposed ES device was then measured while varying the resistive loads, which were simulated to represent different conditions of human tissues. The load conditions were set at 500, 1000, and 2000 ohms, respectively—a range typical of human tissue impedance, as reported by [1].

We then compared the output currents from the proposed ES device and calculated the percentage error (also referred to as percentage deviation) in amplitude using the same formula as in Equation (2). This allowed us to quantify the deviation between the 500-to-1000-ohm load conditions, as well as between the 500-to-2000-ohm load conditions. The primary focus was on observing the percentage amplitude deviation between these two pairs of experiments. A lower percentage of deviation between the two load conditions indicates greater stability in the device's ability to maintain a constant output current, demonstrating its capability to deliver the desired current despite variations in load resistance.

In addition to amplitude comparisons, the stability of the constant output current was further evaluated by analyzing the correlation between the current waveforms from the two pairs of load configurations. Raw data of the arbitrary output waveforms were collected as comma-separated value (CSV) files and used to compute the correlation between the two output currents, assessing the similarity in both pulse duration and pulse repetitive frequency under varying load conditions.

To compare the similarity between two discrete current output waveforms, the Pearson correlation coefficient [37,38,44] provides a reliable measure of the linear relationship between the two signals. The Pearson correlation coefficient quantifies how well the variations in one waveform correspond to the variations in another waveform, helping assess their similarity in terms of amplitude, duration, and also repetitive frequency.

The Pearson correlation coefficient r can be calculated as:

$$r = \frac{\sum(y_i - \overline{y})(z_i - \overline{z})}{\sqrt{\sum(y_i - \overline{y})^2 \sum(z_i - \overline{z})^2}} \tag{4}$$

where y_i and z_i are the individual points of the two discrete waveforms, $\overline{y}$ and $\overline{z}$ are the mean values of the respective waveforms, and r ranges from -1 to 1, where

$r = 1$ indicates a perfect positive correlation,
$r = -1$ indicates a perfect negative correlation,
$r = 0$ indicates no correlation.

By calculating the Pearson correlation coefficient, we assessed the degree of similarity between the two current output waveforms, with higher values of coefficient r indicating a greater similarity in their patterns. Additionally, the Pearson correlation coefficient was employed to explore the interdependencies between key variables—pulse amplitude, pulse duration, and pulse repetitive frequency—to evaluate how changes in one variable may affect another. The results revealed a strong correlation between these parameters, indicating a significant relationship among them. This finding provides valuable insight into the broader performance and interaction of the system's variables.

These two comprehensive analyses ensured that the stability of the proposed ES device was not only assessed in terms of pulse amplitude but also in terms of the pulse durations and pulse repetitive frequencies of all 12 essential current patterns, providing a comprehensive evaluation of the system's performance under variable load conditions.

The experimental results presented in Table 5 clearly indicate that the pulse amplitude of the output current varied within a very narrow range, with deviations of less than $\pm 2\%$ regardless of how the load resistance was altered. Additionally, the computed Pearson

correlation coefficient ***r*** between the two test configurations was exceptionally high, with values ranging from 0.9909 to 0.9994. This high correlation suggests that all of the amplitudes, durations, and repetitive frequencies of the output currents remained consistent, even when load conditions were varied [37,38,44].

Table 5. Amplitude deviation and correlation for load variation from 500 Ω to 2000 Ω.

No	Output Current Patterns	Output Current Settings (mA)	Measured Output Currents with Different Load Impedances (mA)			Load Variation from 500 Ω to 1000 Ω		Load Variation from 500 Ω to 2000 Ω	
			500 Ω [1]	1000 Ω [1]	2000 Ω [1]	Amplitude Deviation	Pearson Correlation Coefficient (*r*)	Amplitude Deviation	Pearson Correlation Coefficient (*r*)
1	IG	40	39.86	40.16	40.09	0.75%	0.9932	0.59%	0.9923
2	CG	40	39.76	39.69	39.79	−0.17%	0.9987	0.09%	0.9991
3	MF	70	69.91	69.97	70.44	0.09%	0.9989	0.76%	0.9988
4	DF	70	69.97	69.20	68.96	−1.11%	0.9985	−1.44%	0.9990
5	CP	70	70.19	70.01	69.95	−0.25%	0.9906	−0.34%	0.9909
6	CPid	70	70.16	70.57	71.10	0.59%	0.9985	1.34%	0.9921
7	LP	70	69.97	70.14	70.38	0.25%	0.9994	0.59%	0.9993
8	TF	80	79.91	81.34	80.05	1.79%	0.9905	0.17%	0.9978
9	RF	80	79.23	79.03	80.08	−0.25%	0.9996	1.07%	0.9994
10	ASYM	140	137.96	138.92	139.64	0.69%	0.9945	1.22%	0.9973
11	ASYM-A	140	138.40	139.13	138.64	0.53%	0.9966	0.17%	0.9958
12	SYM	140	138.65	139.62	140.23	0.70%	0.9982	1.14%	0.9982

3.5. Verification of Compliance with IEC Standards for Medical Equipment

The aim of this testing procedure was to verify that the proposed ES device meets the relevant international medical equipment standards and regulatory requirements. Compliance with these standards is essential to ensure the safety, efficiency, and reliability of the ES device in clinical therapeutic applications. A comprehensive evaluation of the device was conducted in strict accordance with established guidelines, including assessments of electrical safety, electromagnetic compatibility (EMC), and performance benchmarks, to confirm that the proposed ES device meets all necessary criteria for safe and effective operation in real-world ES applications.

The proposed ES device successfully underwent the process of obtaining international certification in accordance with the medical equipment standards including IEC 60601-1 [45], IEC 60601-1-2 [46] and IEC 60601-2-10 [36]. These certifications were conducted by the PTEC, Thailand, a government agency responsible for testing electrical and electronic equipment. The device was certified as meeting the requirements specified by those standards, as documented in the reports [41–43]. The following list of certified standards and corresponding details is provided below.

3.5.1. IEC 60601-1: 2012 (General Requirements for Basic Safety and Essential Performance)

The verification conducted in accordance with this standard include all clauses.

3.5.2. IEC 60601-1-2: 2014 (General Requirements for Basic Safety and Essential Performance—Collateral Standard: Electromagnetic Disturbances)

The verification conducted in accordance with this standard included the following:

- Conducted emission;
- Radiated emission;
- Harmonics emission;
- Voltage fluctuation;
- Electrostatic discharge;

- Radiated RF electromagnetic field immunity;
- Electrical fast transient;
- Electrical surge tolerance;
- Conducted immunity;
- Power frequency magnetic;
- Voltage dips.

3.5.3. IEC 60601-2-10: 2012 (Amendment 2, Particular Requirements for the Basic Safety and Essential Performance of Nerve and Muscle Stimulators)

The verification conducted in accordance with this standard included the following:

- Identification, marking and documents;
- Accuracy of controls and instruments;
- Pulse parameters;
- Protection against hazardous output;
- Supply voltage fluctuations;
- Limitation of output parameters.

Conformity with these three IEC standards ensures that the proposed ES device operates reliably and safely in environments with electromagnetic disturbances, without interfering with the functionality of other devices. Additionally, it demonstrates that the device delivers electrical stimulation output within safe limits, thereby safeguarding patients from potential hazards associated with electrical currents [36,41–43,45,46].

4. Discussion

4.1. Performance and Therapeutic Outcomes

The accuracy of the pulse generator in our proposed device is a critical aspect of performance, particularly when compared to other systems on the market or in previous studies. However, direct comparisons of accuracy are challenging due to the limited availability of detailed data on output current accuracy in existing publications and commercial reports. Most studies focus on operating ranges, such as pulse amplitude, duration, and frequency, without specifying exact accuracy.

For example, Bosques et al. [26] reviewed 37 articles on therapeutic electrical stimulation (ES) and reported effective frequency ranges for NMES, FES, TENS, and TES between 10 and 150 Hz, with pulse durations ranging from 50 to 1000 µs. Broderick et al. [6] examined seven commercial surface-type ES devices, noting frequency ranges from 1 to 140 Hz and pulse durations between 50 and 250,000 µs. Wu et al. [1] developed a multi-channel ES system with frequency ranges of 3–100 Hz and pulse duration adjustability from 50 to 1000 µs, while Chang et al. [12] proposed a microprocessor-based ES device with output currents between −3 and 3 mA, frequency ranges from 10 to 500 Hz, and pulse duration from 50 to 2000 µs.

In comparison, our proposed ES device offers significantly enhanced performance, with a frequency adjustability range of 0.2–1000 Hz and pulse durations from 20 to 1,000,000 µs. Additionally, our device incorporates special functions like Surge and Modulation, which few other devices offer [40]. These functions allow the generation of twelve essential waveforms specifically tailored for various therapeutic needs. Moreover, the device is compliant with IEC 60601-2-10 standards, ensuring that pulse parameter accuracy meets regulatory thresholds, providing confidence in its reliability and performance.

Our device offers significant improvements over existing systems in two key areas:

Performance: The device achieves high levels of accuracy and reliability by complying with all relevant IEC standards, specifically Sections 3.5.1–3.5.3, ensuring precise and consistent output. Additionally, its wide range of adjustability in pulse amplitude, duration, and frequency allows for greater flexibility, enabling a broader range of therapeutic applications compared to other devices on the market.

Therapeutic Outcomes: The combination of enhanced accuracy, flexibility, and adaptability makes the device more effective in delivering treatments across various clinical

settings, including hospitals, clinics, and other healthcare facilities. This versatility ensures that the device can meet the diverse therapeutic needs of patients, making it suitable for a wide range of treatment protocols.

4.2. User Interface and Practical Implementation

The user interface (UI) of our therapeutic electrical stimulator was designed with ease of use and efficiency in mind. The graphical user interface (GUI) features intuitive, touch-based controls that allow clinicians to quickly select waveforms, adjust treatment modes, and modify parameters as needed. Real-time feedback is provided through visual indicators, enabling clinicians to monitor therapy progress and make necessary adjustments without interrupting treatment.

Preliminary usability tests with clinicians have yielded positive feedback. The system was noted to be intuitive and easy to operate, even for users with minimal training. The ability to adjust parameters mid-treatment, such as waveform characteristics or pulse intensity, was highlighted as particularly beneficial in clinical settings. Future usability testing will further assess the UI's performance across a wider range of clinical environments, with the goal of refining the interface to improve the user experience and reduce setup times.

4.3. Power Consumption and Miniaturization

The design of this therapeutic electrical stimulator is optimized for stationary use in clinical environments such as hospitals and clinics, where a stable power supply is available. Consequently, power efficiency and miniaturization were not primary concerns in this study. Instead, the focus was placed on ensuring accuracy and reliability in the device's therapeutic output. However, for future iterations of this device, particularly if portable or wearable versions are considered, power management and miniaturization will become key factors to address.

4.4. Limitations

While the results of this study demonstrate the effectiveness of the proposed therapeutic electrical stimulator, there are several limitations. First, the device was primarily tested under controlled laboratory conditions, and additional clinical trials are required to validate its performance across diverse patient populations and real-world clinical environments. Expanding trials to include a more varied demographic will be essential for assessing the device's efficacy in different therapeutic contexts.

Second, while preliminary tests suggest that the user interface is intuitive, comprehensive usability trials are necessary to ensure that clinicians with varying levels of technical expertise can effectively operate the device. Future development should focus on refining the user interface and creating comprehensive training protocols for clinical staff.

Lastly, while the special functions Surge and Modulation were incorporated based on input from physiotherapists and doctors, further investigation is needed to assess their long-term benefits compared to standard modes. Additional studies are required to evaluate these features across a broader range of clinical conditions to determine their clinical superiority.

4.5. Future Directions

Future work will focus on expanding clinical trials to include a wider range of patient populations to assess the device's performance across various demographics and therapeutic applications. Broader testing will provide further insights into the device's generalizability and ensure its effectiveness in diverse clinical environments. Additionally, future development may involve enhancing the device's usability, power efficiency, and adaptability, especially for potential portable or wearable versions.

5. Conclusions

This study presented the design and successful implementation of a two-channel, multi-functional therapeutic electrical stimulator tailored for clinical applications. The device's capabilities were demonstrated through the generation of twelve essential therapeutic waveforms and two special functions, Surge and Modulation, providing enhanced flexibility and precision in therapeutic treatments. By utilizing an advanced R-2R ladder DAC and an optimized driving stage unit, the proposed device ensured accurate and consistent output across varying load conditions, thereby meeting the stringent safety and performance requirements outlined by the IEC 60601 standards [36,45,46].

Our experimental results validate the device's ability to maintain stable output currents, demonstrating high levels of accuracy, minimal deviation, and adherence to international medical equipment standards. The system's adjustability in pulse amplitude, duration, and frequency, coupled with the integration of special functions, positions it as a versatile tool for a wide range of therapeutic applications, from pain management to muscle rehabilitation. Furthermore, the use of in-house technology and locally sourced components ensures that the device is both cost-effective and accessible, making it particularly suitable for resource-limited healthcare settings.

Overall, the proposed device not only advances the field of therapeutic electrical stimulation but also provides a practical, reliable, and adaptable solution for clinical environments. Future research will focus on broader clinical trials to assess the device's performance across diverse patient populations, further refining its usability and expanding its potential applications in physiotherapy and rehabilitation.

Author Contributions: Conceptualization, C.C.-i., S.B. and R.L.; methodology, R.L., S.B. and C.C.-i.; software, R.L.; validation, R.L. and S.B.; formal analysis, R.L., S.B. and C.C.-i.; investigation, R.L. and S.B.; resources, R.L., S.B. and C.C.-i.; data curation, R.L., S.B. and C.C.-i.; writing—original draft preparation, R.L., S.B. and C.C.-i.; writing—review and editing, R.L. and C.C.-i.; visualization, R.L., S.B. and C.C.-i.; supervision, C.C.-i.; funding acquisition, R.L. and C.C.-i. All authors have read and agreed to the published version of the manuscript.

Funding: This work was supported by King Mongkut's Institute of Technology Ladkrabang (KMITL) under KMITL Doctoral Scholarship Year 2020 (Contract No. KDS2020/003).

Data Availability Statement: The datasets presented in this article are not readily available due to institutional policies. Requests for access to the datasets should be directed to the corresponding author.

Acknowledgments: The authors would also like to thank Boon Supply Co., Ltd. and Thai C Medtech Co., Ltd. for their willing contributions of knowledge, equipment, and supporting teams.

Conflicts of Interest: The authors declare no conflicts of interest.

References

1. Han-Chang, W.; Shueun-Tsong, Y.; Te-Son, K. A versatile multichannel direct-synthesized electrical stimulator for FES applications. *IEEE Trans. Instrum. Meas.* **2002**, *51*, 2–9. [CrossRef]
2. Cheng, K.W.E.; Yan, L.; Kai-Yu, T.; Rad, A.B.; Chow, D.H.K.; Sutanto, D. Development of a circuit for functional electrical stimulation. *IEEE Trans. Neural Syst. Rehabil. Eng.* **2004**, *12*, 43–47. [CrossRef] [PubMed]
3. Velloso, J.B.; Souza, M.N. A Programmable System of Functional Electrical Stimulation (FES). In Proceedings of the 29th Annual International Conference of the IEEE Engineering in Medicine and Biology Society, Lyon, France, 23–26 August 2007; pp. 2234–2237.
4. Forneiro, Y.; Cartaya, M.E.; Folgueras, J.; Colorado, O.; Garcia, J.A.; Rodriguez, A.; Alfonso, L.M.; Lopez, M.; Benitez, R. Therapeutic electrical stimulator. In Proceedings of the 25th Annual International Conference of the IEEE Engineering in Medicine and Biology Society, Cancun, Mexico, 17–21 September 2003; pp. 1716–1719.
5. Xu, Q.; He, J.; Wang, Y.; Xu, T.; Huang, J. A versatile microprocessor-based multichannel stimulator for experimental use in epidural spinal cord stimulation. In Proceedings of the First International Conference on Neural Interface and Control, Wuhan, China, 26–28 May 2005; pp. 205–208.
6. Broderick, B.; Breen, P.; ÓLaighin, G. Electronic stimulators for surface neural prosthesis. *J. Autom. Control* **2008**, *18*, 25–33. [CrossRef]

7. Soedirdjo, S.D.H.; Hutabarat, M.T. Microcontroller-based Transcutaneous Electrical Nerve Stimulator with 8 bit cascade DAC. In Proceedings of the International Conference on Instrumentation, Communication, Information Technology, and Biomedical Engineering, Bandung, Indonesia, 23–25 November 2009; pp. 1–5.
8. Yochum, M.; Binczak, S.; Bakir, T.; Jacquir, S.; Lepers, R. A mixed FES/EMG system for real time analysis of muscular fatigue. In Proceedings of the Annual International Conference of the IEEE Engineering in Medicine and Biology, Buenos Aires, Argentina, 31 August–4 September 2010; pp. 4882–4885.
9. Khosravani, S.; Lahimgarzadeh, N.; Maleki, A. Developing a stimulator and an interface for FES-cycling rehabilitation system. In Proceedings of the 18th Iranian Conference of Biomedical Engineering (ICBME), Tehran, Iran, 14–16 December 2011; pp. 175–180.
10. Qu, H.; Wang, T.; Hao, M.; Shi, P.; Zhang, W.; Wang, G.; Lan, N. Development of a network FES system for stroke rehabilitation. In Proceedings of the 33rd Annual International Conference of the IEEE Engineering in Medicine and Biology Society, Boston, MA, USA, 30 August–3 September 2011; pp. 3119–3122.
11. Masdar, A.; Ibrahim, B.S.K.K.; Jamil, M.M.A. Development of wireless-based low-cost current controlled stimulator for patients with spinal cord injuries. In Proceedings of the IEEE-EMBS Conference on Biomedical Engineering and Sciences, Langkawi, Malaysia, 17–19 December 2012; pp. 493–498.
12. Chang, G.C. A microprocessor-based multichannel subsensory stochastic resonance electrical stimulator. In Proceedings of the 35th Annual International Conference of the IEEE Engineering in Medicine and Biology Society (EMBC), Osaka, Japan, 3–7 July 2013; pp. 3559–3562.
13. Wang, H.P.; Wang, Z.G.; Lü, X.Y.; Huang, Z.H.; Zhou, Y.X. Design of a pulse-triggered four-channel functional electrical stimulator using complementary current source and time division multiplexing output method. In Proceedings of the 37th Annual International Conference of the IEEE Engineering in Medicine and Biology Society (EMBC), Milan, Italy, 25–29 August 2015; pp. 1671–1674.
14. Bhoyania, K.; Bhatt, C.B.; Panchal, C. Multichannel Programmable Functional Electrical Stimulator using Atmega Controller. *Int. J. Eng. Trends Technol.* **2017**, *45*, 424–427. [CrossRef]
15. Ward, T.; Grabham, N.; Freeman, C.; Wei, Y.; Hughes, A.-M.; Power, C.; Tudor, J.; Yang, K. Multichannel Biphasic Muscle Stimulation System for Post Stroke Rehabilitation. *Electronics* **2020**, *9*, 1156. [CrossRef]
16. Khan, A.; Li, K.; Wei, N. Integrated Design of Functional Electrical Stimulator and Transcutaneous Electrical Nerve Stimulator on a Single Prototype. In Proceedings of the 6th IEEE International Conference on Advanced Robotics and Mechatronics (ICARM), Chongqing, China, 3–5 July 2021; pp. 453–458.
17. Wang, J.; Zhang, Y. Design of functional electrical stimulator for foot drop rehabilitation. *J. Phys. Conf. Ser.* **2021**, *1885*, 052005. [CrossRef]
18. Alam, M. An easy-to-build transcutaneous electrical stimulator for spinal cord stimulation therapy, PREPRINT (Version 1). *Res. Sq.* **2022**. [CrossRef]
19. Das, H.; Park, H. MCU-less biphasic electrical stimulation circuit for miniaturized neuromodulator. *Biomed. Eng. Lett.* **2022**, *12*, 285–293. [CrossRef] [PubMed]
20. Slepyan, A.; Krishnan, S.; Li, T.; Thakor, N. A Multi-Channel, Low-Voltage, High-Frequency Programmable Electrical Stimulator for Sensory Feedback. In Proceedings of the IEEE Biomedical Circuits and Systems Conference (BioCAS), Toronto, ON, Canada, 19–21 October 2023; pp. 1–5.
21. Chen, M.; Wu, B.; Lou, X.; Zhao, T.; Li, J.; Xu, Z.; Hu, X.; Zheng, X. A self-adaptive foot-drop corrector using functional electrical stimulation (FES) modulated by tibialis anterior electromyography (EMG) dataset. *Med. Eng. Phys.* **2013**, *35*, 195–204. [CrossRef] [PubMed]
22. Lertsinthai, P. *Electrotherapy for Physical Therapists*, 1st ed.; Naresuan University Publishing House: Phisanulok, Thailand, 2019.
23. Parodi, A.; Choi, J.-W. A Pulse Generation Circuit for Studying Waveform Effects on Neurostimulation. *Electronics* **2019**, *8*, 1344. [CrossRef]
24. Lyons, G.M.; Sinkjaer, T.; Burridge, J.H.; Wilcox, D.J. A review of portable FES-based neural orthoses for the correction of drop foot. *IEEE Trans. Neural Syst. Rehabil. Eng.* **2002**, *10*, 260–279. [CrossRef] [PubMed]
25. Souza, D.; Gaiotto, M.; Nogueira-Neto, G.; Castro, M.C.; Nohama, P. Power amplifier circuits for functional electrical stimulation systems. *Res. Biomed. Eng.* **2017**, *33*, 144–155. [CrossRef]
26. Bosques, G.; Martin, R.; McGee, L.; Sadowsky, C. Does therapeutic electrical stimulation improve function in children with disabilities? A comprehensive literature review. *J. Pediatr. Rehabil. Med.* **2016**, *9*, 83–99. [CrossRef] [PubMed]
27. Lakatem, R.; Leelajindakrairerk, M.; Potivejakul, S.; Sarikprueck, P.; Chompoo-inwai, C. The Conceptual Design and a Partial Development of a Multi-Function Therapeutic Stimulator. In Proceedings of the International Conference on Electrical Engineering, Okinawa, Japan, 3–7 July 2016; pp. 2611–2616.
28. Lakatem, R.; Boontaklang, S.; Chompoo-inwai, C. The 2nd Stage Design and Development of a Two-Channel and Multi-Function Therapeutic Electrical Stimulator Prototype for a Smart Aging Society. In Proceedings of the 24th International Conference on Electrical Engineering, Seoul, Republic of Korea, 24–28 June 2018; pp. 1862–1867.
29. Efstathiou, K.; Karadimas, D. An R-2R ladder-based architecture for high linearity DACs. In Proceedings of the 2007 IEEE Instrumentation & Measurement Technology Conference IMTC 2007, Warsaw, Poland, 1–3 May 2007; pp. 1–5.
30. AnalogDevice. AD826 High-Speed, Low-Power Dual Operational Amplifier. 2010. Available online: https://www.analog.com/en/products/ad826.html#part-details (accessed on 25 June 2023).

31. TexasInstrument. DAC725 Dual 16 bit Digital to Analog Converter. 1993. Available online: https://mou.sr/4gDKBB9 (accessed on 25 June 2023).
32. Johnny Guo, D.L. *Design a Flybuck Solution With Optocoupler to Improve Regulation Performance*; Texas Instruments: Dallas, TX, USA, 2015.
33. Robinson, A.J.; Snyder-Mackler, L. *Clinical Electrophysiology: Electrotherapy and Electrophysiologic Testing*; Williams & Wilkins: Philadelphia, PA, USA, 1995.
34. Kitchen, S. *Electrotherapy: Evidence-Based Practice*, 11th ed.; Churchill Livingstone: Edinburgh, UK; New York, NY, USA, 2002.
35. Walsh, D.M.; Howe, T.E.; Johnson, M.I.; Moran, F.; Sluka, K.A. Transcutaneous electrical nerve stimulation for acute pain. *Cochrane Database Syst. Rev.* **2009**. [CrossRef]
36. *IEC 60601-2-10 Standard*; Medical Electrical Equipment—Part 2–10: Particular Requirements for the Basic Safety and Essential Performance of Nerve and Muscle Stimulators. IEC: Geneva, Switzerland, 2012.
37. Kreyszig, E. *Advanced Engineering Mathematics*; Wiley: Hoboken, NJ, USA, 2017.
38. Cumming, G.; Calin-Jageman, R. *Introduction to the New Statistics: Estimation, Open Science, and Beyond*, 1st ed.; Routledge: Oxford, UK, 2016.
39. Adel, R.V.d.; Luykx, R.H.J. *Low and Medium Frequency Electrotherapy*; Enraf Nonius B.V.: Rotterdam, The Netherlands, 2005.
40. Enraf-Nonius. 4-Series Operating Instructions. 2023, pp. 57–60. Available online: https://www.enraf-nonius.com/index.php/products/downloads (accessed on 25 June 2023).
41. *Test Report: IEC 60601-2-10 Medical Electrical Equipment—Part 2–10: Particular Requirements for the Basic Safety and Essential Performance of Nerve and Muscle Stimulators*; 163/64-001; Electrical and Electronic Products Testing Center (PTEC): Pathum Thani, Thailand, 2020.
42. *Test Report: IEC 60601-1-2 Medical Electrical Equipment—Part 1-2: General Requirements for Basic Safety and Essential Performance—Electromagnetic Disturbances*; 10/62-96; Electrical and Electronic Products Testing Center (PTEC): Pathum Thani, Thailand, 2020.
43. *Test Report: IEC 60601-1 Medical Electrical Equipment—Part 1: General Requirements for the Basic Safety and Essential Performance*; 80/65-004; Electrical and Electronic Products Testing Center (PTEC): Pathum Thani, Thailand, 2022.
44. Nicewander, J.L.R.W.A. Thirteen Ways to Look at the Correlation Coefficient. *Am. Stat.* **1988**, *42*, 59–66.
45. *IEC 60601-1 Standard*; Medical Electrical Equipment—Part 1: General Requirements for Basic Safety and Essential Performance. IEC: Geneva, Switzerland, 2012.
46. *IEC 60601-1-2 Standard*; Medical Electrical Equipment—Part 1-2: General Requirements for Basic Safety and Essential Performance –Collateral Standard: Electromagnetic Disturbances—Requirements and Tests. IEC: Geneva, Switzerland, 2014.